Power Electronics and Drives
Volume 10(45), 2025 DOI: 10.2478/pead-2025-0012

sciendo

Power Electronics and Drives

# Energy Optimal Control of Electromechanical Systems: Trade-off Demands

**Research Paper**

Branislav Ftorek[1], Vladimír Vavrúš[2,*], Ján Šimon[1], Ján Vittek[1]

[1]Department of Applied Mathematics, Faculty of Mechanical Engineering, University of Žilina, 010 26 Žilina, Slovakia
[2]Department of Power Systems and Electric Drives, Faculty of Electrical Engineering and Information Technology, University of Žilina, 010 26 Žilina, Slovakia

**Received: 03 March, 2025; Received in the revised form: 13 May, 2025; Accepted: 27 May, 2025**

**Abstract:** This study presents research on the impact of the selection of the required manoeuvre time on the energy consumption of an electromechanical system, using the example of a train. Two different energy conservation control strategies [energy optimal control (EOC) and energy near-optimal control (ENOC)] were applied to assess their consumption as a function of recommended travel time. The optimal control variables are provided by an energy-saving reference position generator, whose outputs are then faithfully followed using a feedback control based on field orientation, and this is accomplished with a matched zero dynamic lag pre-compensator, yielding the required closed-loop dynamics. The load torque, consisting of constant, linear and quadratic components as a function of speed, is treated as a state variable. The potential for energy savings by reducing the speed of such systems was verified through MATLAB simulations. As a representative controlled electromechanical system, a suburban train unit was chosen for simulations to evaluate the energy consumption of both control approaches.

**Keywords:** *Energy near-optimal position control • field-oriented control • dynamic lag pre-compensator • train position control*

## 1. Introduction

The driving strategy of electromechanical systems has a significant influence on their energy consumption. The original control strategies, which relied on maximum acceleration and speed, were highly energy-demanding. This prompted the development of energy-efficient control methods. These methods can significantly reduce the drive's energy consumption, improving environmental sustainability and lowering operational costs.

To verify the effect of practicable manoeuvre time selection, this study presents two different control strategies that are capable of minimising the drive's electrical and mechanical losses. The first strategy, energy optimal control (EOC), is based on the Euler-Lagrange principle approach (Pontryagin, 2018), while the second strategy, energy near-optimal control (ENOC), is based on the prediction of drive losses (Tolle, 1975). ENOC exploits a symmetrical trapezoidal speed profile with truly finite settling time. Both position control strategies are designed to complete a position manoeuvre in the prescribed manoeuvre time ($T_m$). The description of the route between two stops, including passive resistance to the movement of a given system, is required for the design of optimal energy-saving output state variables. The value of the average gradient of the route is added to the constant train resistance to avoid the computation of necessary switching points for changing the slope on the route. Regenerative braking is assumed for both control strategies. The energy-saving reference position generator produces optimal time functions of position, speed and acceleration between two stops. These outputs are then faithfully followed using a feedback control based on field orientation (Novotny and Lipo, 1996) and accomplished with a matched zero dynamic lag pre-compensator, yielding the required closed-loop dynamics.

* *Email: vladimir.vavrus@uniza.sk*

Possible energy savings through minimising the drive's speed depend on load torque, which can consist of constant (Coulomb), linear (viscous) and quadratic (drag coefficient) components. Propelling mechanisms with typical linear friction have a load torque directly proportional to the angular speed ($\omega$). The power as a product of torque and speed is proportional to the square of speed ($\omega^2$). By halving the drive's speed to $\omega/2$, energy demands are reduced by 50% compared with the original speed requirements, despite the manoeuvre time being twice as long [Eq. (1a)].

Higher energy savings can be achieved by halving the speed of mechanisms with quadratic torque (such as pumps and fans), where the load torque is proportional to the square of the speed ($\omega^2$). In this case, power is proportional to $\omega^3$, and by halving the drive's speed to $\omega/2$, energy demands are reduced by 75% compared with the original speed requirements, despite the manoeuvre time being twice as long [Eq. (1b)].

$$\frac{\omega^2 T - (\omega/2)^2\, 2T}{\omega^2 T} 100 = 50\% \tag{1a}$$

$$\frac{\omega^3 T - (\omega/2)^3\, 2T}{\omega^3 T} 100 = 75\% \tag{1b}$$

These two examples of load torque influence on energy consumption offer a general conclusion: the maximum speed of electromechanical systems should be kept to the minimum practicable value. Since the load torque of most drives includes all three aforementioned components, choosing a practical manoeuvre time significantly impacts both energy consumption and the balance between the drive's cost and users' benefits.

The increasing demand for energy-saving technologies is reflected in numerous researches dedicated to this subject. The first application of Pontryagin's maximum principle (PMP) to train operations dates back to 1968 (Ichikawa, 1968). The developed train and route model was restricted to a flat track and a load torque containing only a linear component.

To solve the problem of finding the optimal control strategy for trains equipped with diesel-electric locomotives, a combination of two different approaches was proposed (Howlett, 2000). For continuous control problems, PMP is used, while for discrete control issues, which are common in diesel-electric locomotive fuel consumption, optimal switching times are determined by utilising the Kuhn-Tucker conditions to minimise fuel usage.

The PMP approach is also used to derive energy-optimal trajectories by Heineken et al. (2023). A special code, Leda, was developed to construct the unique minimum energy trajectories as the solution. As an example of energy savings, the sensitivity to deviations of the train speed from the calculated optimal speed profile is studied in detail.

Several models and numerical algorithms were developed for traction applications to minimise losses of traction drives by adjusting switching points for the complete optimal trajectory design.

An algorithm optimising the driving style of a train, enabling energy optimisation, is described by Franke et al. (2000). A non-linear point-mass model of the train, incorporating the motion equation, is arranged to facilitate a piecewise analytical solution to the non-linear control problem. This designed algorithm creates a suitable base for a non-linear model predictive controller to operate in real-time.

An optimal control algorithm for the reduction of energy consumption of subway trains based on proximal policy optimisation (PPO) is proposed by Chen et al. (2023). The reinforcement learning architecture model for optimal control of the train is constructed as the first step. This model is then trained by exploiting PPO and reward scaling. As a result, the effective reduction of train energy consumption was achieved.

A new cellular automation model of train movement under mixed-traffic conditions and loss minimisation is proposed by Ping et al. (2023). The space-time diagram of the existing traffic flow is investigated, as well as the train movement, to obtain updated rules for the driver of the train.

A complex analysis of the operation strategies and their impact on the overall system design of the metro train is described by Su et al. (2016). The optimal train control model considers parameters, such as train mass reduction, minimising traction resistances, designing energy-saving gradients and implementing regenerative braking, along with corresponding timetable optimisation. An optimal train control simulator, based on an energy-efficient system, enables the analysis of practical operational data from the Beijing metro line. Quantitative analysis of possible energy reduction for different vehicle parameters and control strategies helps the decision-makers to adjust the balance between system costs and passenger benefits.

To investigate the influence of manoeuvre time selection on energy demands, the simulation of the suburban train unit propelled by induction motors was chosen as an example. The results gained are valid for any electric drive load torque that is speed-dependent, as described further. The control system of this unit, shown in Figure 1, exploits principles of field-oriented control (FOC) due to its fast dynamic response and the possibility of controlling torque and field components of stator current separately (Orlowska-Kowalska and Dybkowski, 2016; Perdukova et al., 2004). The FOC technique also offers significant potential for a considerable reduction of drive losses.

The mathematical description of the control system for optimising the drive's energy consumption consists of four differential equations that account for vehicle dynamics as well as the traction motor (TM) position, speed and current dynamics (Brandstetter and Dobrovsky, 2013). The resulting energy-saving speed profiles consist of the following modes: acceleration, cruising and braking. The designed control structure for verification is shown in Figure 1 and consists of an EOC or ENOC energy saving profile generator (position, speed, acceleration and jerk) accomplished with zero-lag pre-compensator and a position-controlled induction TM capable of precise tracking of generated state variables (Vittek et al., 2017a,b).

## 2. Theoretical Background

In previous work (Ftorek et al., 2021; available as Open Access Journal), the background of EOC and ENOC for rotational drives was described in detail. Therefore, only the parts necessary for the implementation of these control strategies are listed further.

The movement of the suburban train unit is described by the following differential Eq. (2):

$$m_t \frac{\mathrm{d}^2 S_{TD}}{\mathrm{d}t^2} = F_t(t,v) - F_p(v) - F_s(S_{TD}) - F_b(v) \tag{2}$$

where $m_t$ is the total mass of the train, $S_{TD}$ is the travel distance between two stops, $F_t$ is the traction force, $F_p$ is the force covering vehicle resistance, $F_s$ is the force covering slope resistance and $F_b$ is the braking force, respectively.

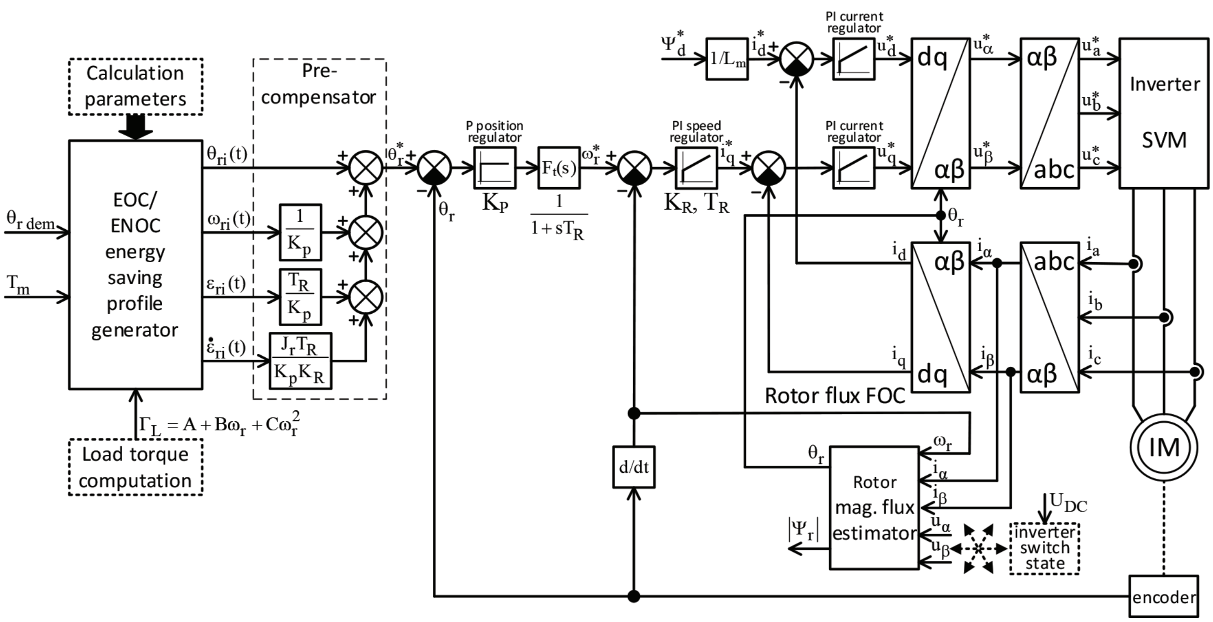


**Figure 1.** Overall control system for verification of energy-saving control of train unit with induction motors. ENOC, energy near-optimal control; EOC, energy optimal control; FOC, field-oriented control.

The relationship between travel distance ($S_{TD}$) and TM rotor position $\theta_r$ is given in Eq. (3):

$$\theta_r = \frac{2u}{D_{wa}} S_{TD} \tag{3}$$

where $D_{wa}$ is the average diameter of the driving wheel, and $u$ is the gear ratio between the rotor of TM and the driving wheel. The following Eq. (4) determines TM rotational speed ($\omega_r$) as a function of vehicle velocity ($v_V$)

$$\omega_r = \frac{u}{1.8D_{wa}} v_V. \tag{4}$$

Constant, linear and quadratic traction resistances to unit movement as a function of vehicle speed are defined in Eq. (5):

$$p_0 = A + Bv_V + Cv_V^2 \tag{5}$$

and for suburban unit has form $p_0 = 3.1 + 0.025v_V + 0.00038v_V^2$. The relationship between TM torque ($\Gamma_{\mathrm{TM}}$) and train unit traction force ($F_t$) is given in Eq. (6).

$$\Gamma_{TM} = \frac{D_{wa}}{2mu} F_t \tag{6}$$

The parameters of the train unit are listed in Table A1 in the Appendix. By analysing these strategies, this study aims to evaluate their effectiveness in minimising energy consumption while maintaining optimal operational performance.

## 2.1. EOC

EOC is based on Euler–Lagrange optimisation. The dynamical system for optimisation of AC drives [Eqs (7) and (8)] consists of the differential equations for rotor position ($\theta_r$), rotor speed ($\omega_r$) and electric torque ($\Gamma_e$). In Eq. (7), $J_r$ stands for the moment of inertia reduced to the shaft. The load torque ($\Gamma_L$) is treated as the state variable; therefore, the system is completed with its derivative, which is the function of rotor speed. The load torque can be written as the sum of the constant term $A$, linear term $B\omega_r$ and quadratic component $C\omega_r^2$. The time derivative of the load torque has the form: $\dot{\Gamma}_L = (B + 2C\omega_r)\dot{\omega}_r$.

$$\begin{bmatrix} \dot{\theta}_r \\ \dot{\omega}_r \\ \dot{\Gamma}_e \\ \dot{\Gamma}_L \end{bmatrix} = \begin{bmatrix} 0 & 1 & 0 & 0 \\ 0 & 0 & 1/J_r & -1/J_r \\ 0 & -k_\omega & -k_\Gamma & 0 \\ 0 & 0 & (B+2C\omega_r)/J_r & -(B+2C\omega_r)/J_r \end{bmatrix} \begin{bmatrix} \theta_r \\ \omega_r \\ \Gamma_e \\ \Gamma_L \end{bmatrix} + \begin{bmatrix} 0 \\ 0 \\ k_U \\ 0 \end{bmatrix} u_q \tag{7}$$

$$y = [1 \quad 0 \quad 0 \quad 0][\theta_r \quad \omega_r \quad \Gamma_e \quad \Gamma_L]^{\mathrm{T}} \tag{8}$$

Constants of Eq. (7) for the IM are defined as: $R_c = R_s + R_r (L_m/L_r)^2$, $k_\Gamma = R_c/\sigma L_s$, $k_\omega = pk_t\Psi_D(c_2/\sigma L_s + 1/L_m)$ and $k_U = k_t/\sigma L_s$. The IM torque constant, $k_t = 3pL_m\Psi_D/L_r$ and $u_q$, is the $q$-axis excitation voltage for both motors. For simplification of calculations, a new constant ($k_m$) was defined as $k_m = k_t^2/2R_c$.

If Euler–Lagrange calculus is applied to the system (7), a highly non-linear system (9) is obtained. This system consists of two derivatives of Lagrange coefficients $\lambda_{1,2}$ and the derivative of rotor speed and rotor position, which can only be solved numerically

$$\begin{bmatrix} \dot{\lambda}_1 \\ \dot{\lambda}_2 \\ \dot{\omega}_r \\ \dot{\theta}_r \end{bmatrix} = \begin{bmatrix} B/J_r & -1/J_r & 2B/J_r & 0 \\ 0 & 0 & 0 & 0 \\ k_m/J_r & 0 & -B/J_r & 0 \\ 0 & 0 & 1 & 0 \end{bmatrix} \begin{bmatrix} \lambda_1 \\ \lambda_2 \\ \omega_r \\ \theta_r \end{bmatrix} + \begin{bmatrix} 1/J_r \\ 0 \\ -1/J_r \\ 0 \end{bmatrix} A + \begin{bmatrix} 2C\lambda_1 \\ 0 \\ 0 \\ 0 \end{bmatrix} \omega_r + \begin{bmatrix} 3C/J_r \\ 0 \\ -C/J_r \\ 0 \end{bmatrix} \omega_r^2 \tag{9}$$

The derived system (9) must satisfy boundary conditions (10), which are as follows:

$$\begin{aligned}
&\text{for } t = t_0 \;\rightarrow \qquad && \omega_r(t_0) = \omega_0 \\
& && \theta_r(t_0) = \theta_{r0}, \\
&\text{for } t = T_m \;\rightarrow \qquad && \omega_r(T_m) = \omega_m \\
& && \theta_r(T_m) = \theta_r
\end{aligned} \tag{10}$$

The solution to system (9) with boundary conditions (10) is obtained using the MATLAB function, *bvp4c.m* (*boundary value problem*). By providing approximation points for the expected solution, this solver creates a mesh and determines a numerical solution by solving the differential equations resulting from the boundary conditions and the collocation conditions imposed on all subintervals. Subsequently, the solver estimates the error of the computed solution on each subinterval. If the solution does not meet the tolerance criteria, the solver adapts the mesh and repeats the process. The resulting functions for acceleration, speed and position meet the requirements for minimum energy consumption.

## 2.2. ENOC

The ENOC approach is based on the detailed prediction of copper and friction losses while using the symmetrical trapezoidal profile of rotor speed. The total drive energy [Eq. (11)], including predictable drive losses, is then defined as:

$$W_T = \frac{3}{2}\int_0^{T_m} R_c i_q^2 \, \mathrm{d}t + \int_0^{T_m} \left(A + B\omega_r + C\omega_r^2\right)\omega_r \, \mathrm{d}t \tag{11}$$

After integration over the manoeuvre time $T_{m,}$ as a function of acceleration interval $T_\varepsilon$ for the demanded position setpoint $\theta_{rd}$, the total consumed energy $W_T$ results in Eq. (12):

$$W_T = \frac{\theta_{rd}^2}{\left(T_m - T_\varepsilon\right)^2}\left[\frac{k_1}{T_\varepsilon} + k_s\left(T_m - \frac{4}{3}T_\varepsilon\right) + k_3\frac{\theta_{rd}^2}{\left(T_m - T_\varepsilon\right)^2}\left(T_m - \frac{8}{5}T_\varepsilon\right) + k_5\frac{\theta_{rd}}{\left(T_m - T_\varepsilon\right)}\left(T_m - \frac{3}{2}T_\varepsilon\right)\right] + k_A T_m + k_6\theta_{rd} + A\theta_{rd} \tag{12}$$

where $k_1 = 3R_c\frac{J_r^2}{(c\Psi)^2}$, $k_2 = \frac{3}{2}R_c\frac{A^2}{(c\Psi)^2} + B$, $k_3 = \frac{3}{2}R_c\frac{C^2}{(c\Psi)^2}$, $k_4 = 3R_c\frac{AC}{(c\Psi)^2}$, $k_5 = 3R_c\frac{BC}{(c\Psi)^2} + C$, $k_6 = 3R_c\frac{AB}{(c\Psi)^2}$,

$k_A = \frac{3}{2}R_c\frac{A^2}{(c\Psi)^2}$ and $k_s = k_2 + k_4$.

The optimised acceleration time ($T_{\varepsilon\ opt}$) yielding energy demand minimisation [Eq. (13)] is determined via the derivative: $\mathrm{d}W_T/\mathrm{d}T_\varepsilon = 0$ as:

$$\begin{aligned}
&-\frac{4}{3}k_s T_\varepsilon^5 + \left[\frac{10}{3}k_s T_m + 3k_5\theta_{rd}\right]T_\varepsilon^4 + \left[3k_1 - \frac{2}{3}k_s T_m^2 - \frac{9}{2}k_5\theta_{rd}T_m - \frac{24}{5}k_3\theta_{rd}^2\right]T_\varepsilon^3 + \\
&+\left[-7k_1 + \frac{2}{3}k_s T_m^3 + \frac{3}{2}k_5\theta_{rd}T_m^2 + \frac{12}{5}k_3\theta_{rd}^2 T_m\right]T_\varepsilon^2 + 5k_1 T_m^2 T_\varepsilon - k_1 T_m^3 = 0
\end{aligned} \tag{13}$$

Newton's formula is used to solve this fifth-order algebraic equation and find the optimised acceleration time ($T_{\varepsilon\ opt}$). The near-optimal acceleration time ($T_{\varepsilon\ opt}$) also determines the optimal acceleration ($\varepsilon_{p\ opt}$) as given by Eq. (14):

$$\varepsilon_{p\ opt} = \frac{\theta_{rd}}{T_{\varepsilon\ opt}\left(T_m - T_{\varepsilon\ opt}\right)} \tag{14}$$

During the analysis of energy consumption, it was observed that the drive's cruising speed can be maintained at the minimum practicable values in the presence of any speed-dependent torque components (linear or quadratic), resulting in reduced energy consumption. In contrast, for any combination of these two components with constant friction, there exists only one unique solution for the manoeuvre time ($T_m$).

## 3. Influence of Travel Time on Energy Consumption of Near-Optimal Control

To investigate the influence of travel time on the minimisation of energy consumption, the proposed control strategies were implemented into a traction unit with maximum speed $v_{max}$ = 100 km/h and two induction TMs with a total nominal power of $P_T$ = 1 440 kW, with parameters listed in Table A1 in the Appendix. The overall control system, shown in Figure 1, has a cascade structure and consists of energy-saving profile generators (EOC and ENOC) and a position control system based on FOC (Orlowska-Kowalska and Dybkowski, 2016), completed with a dynamic-lag pre-compensator (Vittek et al., 2017a,b) that ensures precise tracking of prescribed state variables, using near-optimal energy behaviour.

The maximum speed for the ENOC simulations was adjusted to match the maximum speed of the EOC, as shown in Figure 2. The geometry of the symmetrical trapezoidal speed profile was used to adjust the corresponding acceleration time $T_{\varepsilon i}$.

$$T_{\varepsilon i} = T_{mi} - \frac{S_{TD}}{v_{ti}} \tag{15}$$

The computed acceleration times were $T_{\varepsilon 1}$ = 60.932 s, $T_{\varepsilon 2}$ = 62.713 s and $T_{\varepsilon 1}$ = 65.082 s. The simulation results gained for a travel time $T_{m2}$ = 300 s, corresponding to an average speed of 60 km/h, are compared with the results from the other two travel times. Time functions of the prescribed state variables (acceleration, speed and position) for both EOC and ENOC travel times ($T_{m2}$) are shown in Figure 3.

The functions of real control variables, including speed vs. position, speed vs. time, torque current component vs. time and energy consumption vs. time, for both EOC and ENOC are presented in Figures 4 and 5. The energy consumption profiles highlight both the peak value and total energy consumption associated with the entire vehicle, while the torque current component profile pertains to a single TM.

Tables 1 and 2 summarise the chosen maximum and minimum values of current and consumed energy for a given run. Short current switching transients were filtered, while their influence on total energy consumption was retained. The peak energy during the corresponding run is denoted as $W_{max}$. The useful energy delivered to the shaft of the TM to overcome traction resistances is referred to $W_{sh}$. The total energy consumed during a given run is indicated as $W_T$. The difference between $W_{max}$ and $W_T$ represents the recuperated energy during electro-dynamical braking.

Subplot (a) of Figure 4 confirms that the required travel distance ($S_{TD}$ = 5000 m) was reached for all three prescribed travel times. Subplot (b) presents the time functions of the three speed profiles corresponding to the prescribed travel times. Subplot (c) shows the time functions of the current torque components for the TM. Finally,

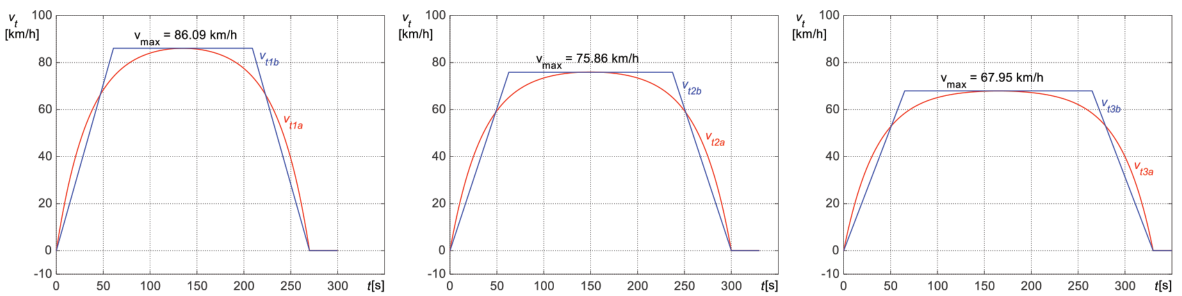


(a) $T_{m1} = 270$ s (b) $T_{m2} = 300$ s (c) $T_{m3} = 330$ s

**Figure 2.** Energy-saving time profiles of the prescribed speed for EOC and ENOC. ENOC, energy near-optimal control; EOC, energy optimal control.

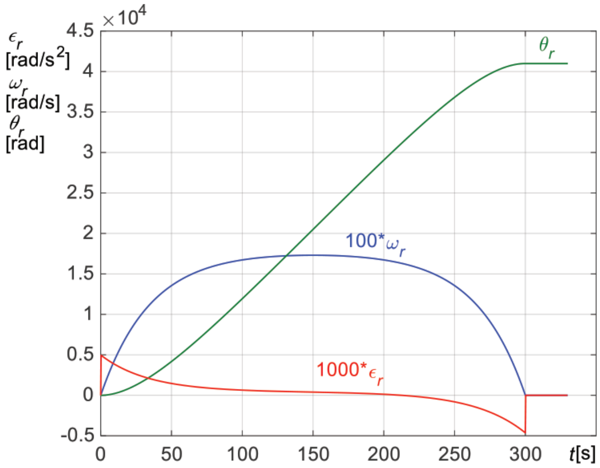


(a) EOC

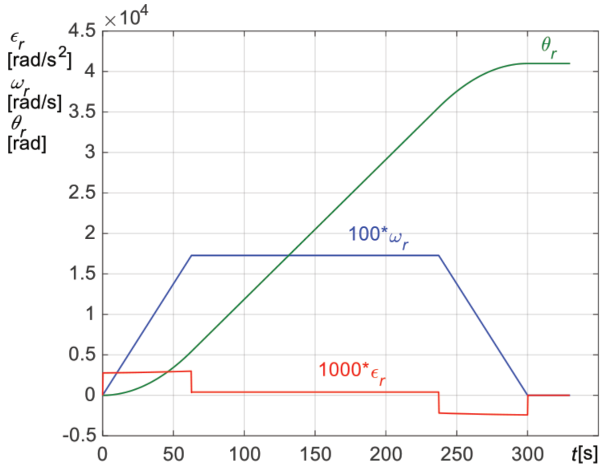


(b) ENOC

**Figure 3.** Prescribed time functions of acceleration, speed and position for $T_{m2}$ = 300 s. ENOC, energy near-optimal control; EOC, energy optimal control.

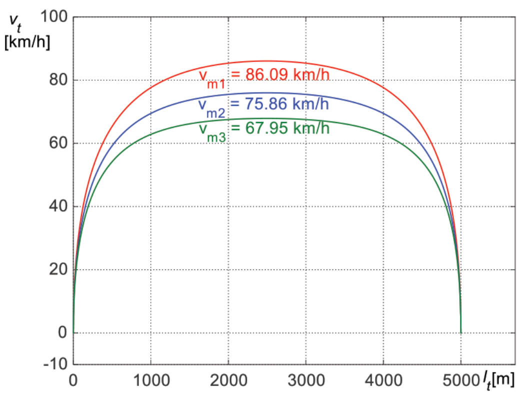


(a) Speed as a function of position

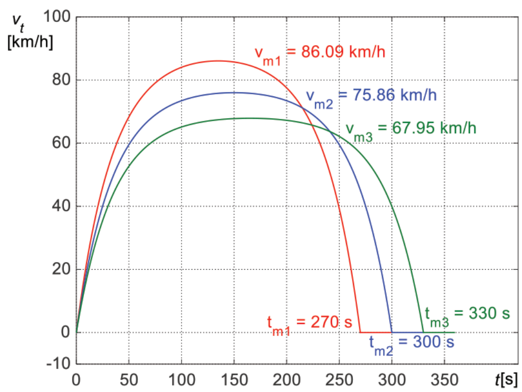


(b) Time functions of speed

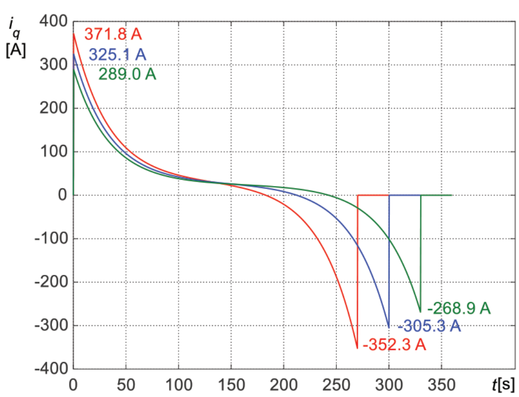


(c) Time functions of the current torque component

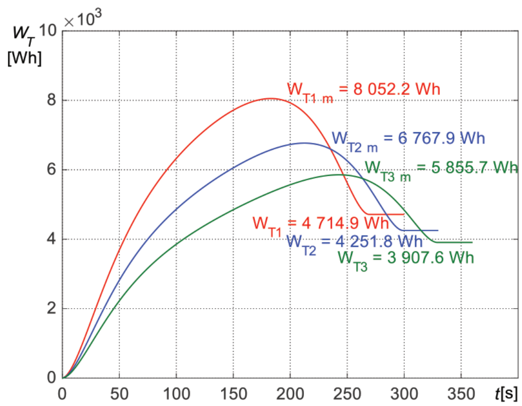


(d) Total energy consumption of the whole unit

**Figure 4.** EOC profiles of speed, current and total energy consumption. EOC, energy optimal control.

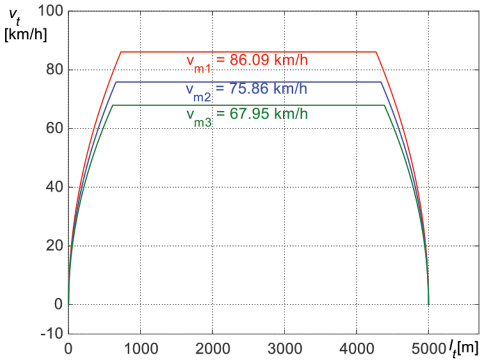


(a) Speed as a function of position

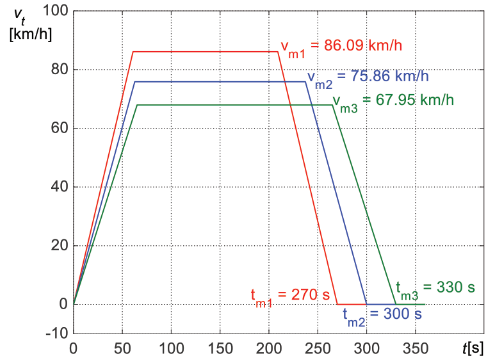


(b) Time functions of speed

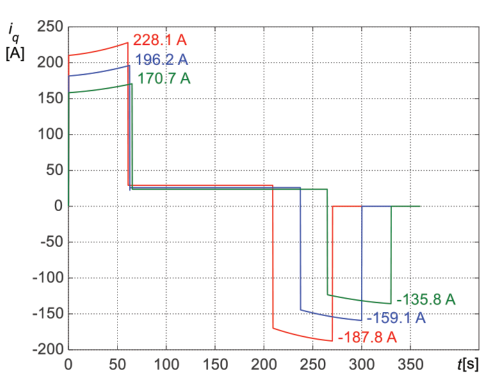


(c) Time functions of the current torque component

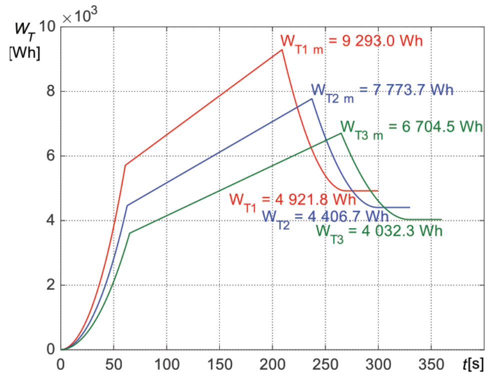


(d) Total energy consumption of the whole unit

**Figure 5.** ENOC profiles of speed, current and total energy consumption. ENOC, energy near-optimal control.

**Table 1.** Peak and minimum values of speed, current and energy for different manoeuvre times under the EOC strategy.

| $V_{max}$ (km/h) | $I_{max}$ (A) | $I_{min}$ (A) | $W_{sh}$ (Wh) | $W_{max}$ (Wh) | $W_T$ (Wh) |
|---|---|---|---|---|---|
| $T_{m1}$ = 270 s | | | | | |
| 86.094 | 371.8 | –352.3 | 4468.2 | 8052.2 | 4714.9 |
| $T_{m2}$ = 300 s | | | | | |
| 75.858 | 325.1 | –305.3 | 4062.8 | 6767.9 | 4251.8 |
| $T_{m3}$ = 330 s | | | | | |
| 67.946 | 289.0 | –268.9 | 3758.0 | 5855.7 | 3907.6 |

EOC, energy optimal control.

**Table 2.** Peak and minimum values of speed, current and energy for different manoeuvre times under the ENOC strategy.

| $V_{max}$ (km/h) | $I_{max}$ (A) | $I_{min}$ (A) | $W_{sh}$ (Wh) | $W_{max}$ (Wh) | $W_T$ (Wh) |
|---|---|---|---|---|---|
| $T_{m1}$ = 270 s | | | | | |
| 86.094 | 228.1 | –187.8 | 4659.4 | 9293.0 | 4921.8 |
| $T_{m2}$ = 300 s | | | | | |
| 75.858 | 196.2 | –159.1 | 4207.3 | 7773.7 | 4406.7 |
| $T_{m3}$ = 330 s | | | | | |
| 67.946 | 170.7 | –135.8 | 3876.7 | 6704.5 | 4032.3 |

ENOC, energy near-optimal control.

subplot (d) shows the total energy consumption $W_T$ as a function of time, along with the peak energy ($W_{max}$). To facilitate the identification of the maximum and minimum values of the selected variables, these values are summarised in Table 1.

If $T_{m2}$ = 300 s is taken as the base for investigating the influence of travel time, a 10% decrease in travel time ($T_{m1}$ = 270 s) results in an increase of 14.36% in the motoring torque current component and 15.39% in the generating torque current component. The magnitude of consumed energy increases by 18.97%, while the total consumed energy increases by 10.89%.

On the contrary, a 10% increase in manoeuvre time ($T_{m3}$ = 330 s) results in a decrease of 11.1% in the motoring torque current component and 11.92% in the generating torque current component. The magnitude of consumed energy decreases by 13.48%, and the total consumed energy decreases by 8.81%.

Additionally, ENOC subplot (a) of Figure 5 confirms that the required travel distance ($S_{TD}$ = 5000 m) was reached for all three prescribed travel times. Subplot (b) shows the time functions of the speed profiles for different travel times. Subplot (c) shows the time functions of the current torque components for a single TM, while subplot (d) displays energy consumption (both peak and total) as a function of time. The maximum and minimum values of the chosen variables for ENOC are summarised in Table 2.

If $T_{m2}$ = 300 s is taken as a baseline, a 10% decrease in travel time ($T_{m1}$ = 270 s) results in a 16.26% increase and a 15.03% increase in the magnitudes of motoring and generating torque current components, respectively. The magnitude of consumed energy increases by 19.54%, and the total consumed energy increases by 11.69%. On the contrary, a 10% increase in manoeuvre time ($T_{m3}$ = 330 s) results in a decrease of 12.99% in the motoring torque current component and 14.64% in the generating torque current component. The magnitude of consumed energy decreases by 13.75%, and the total consumed energy decreases by 8.5%.

The influence of wide-spectrum changes in travel time, due to the necessary numerical solution of the EOC strategy, was limited to ENOC, resulting in 3D graphs that show the effects of such changes.

Consumed energy as a function of prescribed travel time ($T_m$) and corresponding acceleration time ($T_\varepsilon$) is shown in Figure 6. To show the computed real minimum energy consumption graph (6a) extends the coordinates $T_m$ and $T_\varepsilon$ to non-realistic values of 5000 s and 250 s, respectively. The coordinates of the computed minimum energy consumption (marked by the red point) are [$T_{m\ min}$ $T_{\varepsilon\ min}$ $W_{T\ min}$] = [4000.025 s 96.788 s 2104 Wh]. To obtain more realistic travel time values, $T_m$ was halved twice and the corresponding results are summarised in Table 3.

Halving the coordinates $T_m$ and $T_\varepsilon$ twice of the computed energy minimum in Figure 6(a) results in their substantial reduction, bringing them closer to realistic values for manoeuvre time, $T_m$. The corresponding increase in consumed energy is only +2.52% and +14.5%, respectively. To approach real values for travel time $T_m$, the new coordinates in

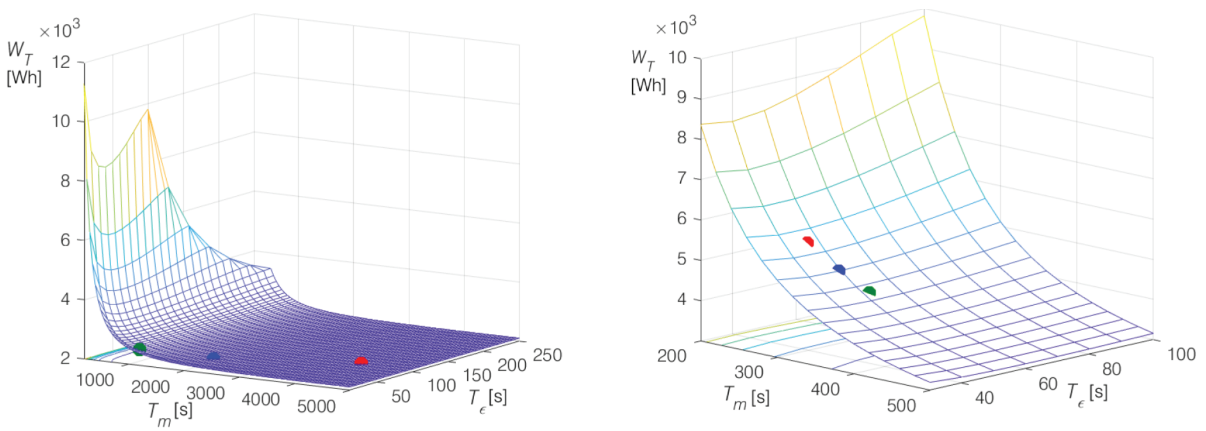


(a) Energy consumption across a wide spectrum for investigating minimum energy consumption

(b) Energy consumption for a limited spectrum assuming real-time applications

**Figure 6.** 3D graph of energy consumption response to variations in manoeuvre time ($T_m$) and acceleration time ($T_\varepsilon$).

**Table 3.** Total consumed energy.

| Point colour | $T_m$ (s) | $T_\varepsilon$ (s) | $W_T$ (Wh) | Energy increase (%) |
|---|---|---|---|---|
| Red (min. point) | 4100.025 | 96.788 | 2104 | 0.0 |
| Blue | 2050.012 | 48.394 | 2157 | +2.52 |
| Green | 1025.006 | 24.197 | 2409 | +14.5 |

Figure 6(b) are significantly limited to [$T_{m\ max}$ $T_{\varepsilon\ max}$ $W_{T\ max}$] = [500 s 100 s 9000 Wh]. Energy consumption, computed for minor changes in travel time $T_m$, is now visible as dots (green, blue and red). It is evident that for shorter times, such as $T_{m3}$ = 270 s, the energy consumption follows a steep slope.

As observed from both the evaluations of minor changes and substantial changes in travel time, a common feature for energy savings is to maintain the maximum speed of electromechanical systems at the minimum practicable values.

# 4. Conclusion

This study presents significant research on electromechanical systems and the potential for energy savings through the choice of prescribed manoeuvre time. As a case study, the movement of a suburban train unit and its energy consumption are evaluated using two different energy-saving control strategies (EOC and ENOC). The train unit control system consists of an energy-saving profile generator, followed by a dynamic-lag pre-compensator, and a position-controlled induction motor drive operating under the principles of FOC. This control structure effectively eliminates dynamic lag, ensuring that pre-computed energy-optimal and near-optimal reference input functions are precisely followed, resulting in ENOC performance by the control system. The potential for experimental implementation of the proposed control strategies under laboratory conditions was presented in previous work.

The comparisons of energy consumption for travel time $T_{m2}$ = 300 s revealed that a 10% increase in travel time ($T_{m3}$ = 330 s) resulted in energy savings of 8.81% for EOC and 8.5% for ENOC.

Conversely, a 10% reduction in travel time $T_{m1}$ = 270 s led to an increase in energy consumption, 10.89% with EOC and 11.69% with ENOC. In conclusion, the evaluation of energy savings confirms that the maximum speed of position-controlled electromechanical systems should be maintained at the minimum practicable level.

The findings of this study are applicable to any electromechanical system that defines the three components of load torque and uses automatic control of torque and speed. The total energy consumption for both control strategies was verified in two ways: first, by integrating the motor input power over time, and second, by summing the individual energy components, including motor losses and the energy delivered to the motor's shaft. Simulation results confirm that the EOC strategy leads to the lowest energy consumption compared with ENOC.

# Acknowledgements

The authors wish to thank the Cultural and Educational Grant Agency of the Ministry of Education, Science, Research and Sport of the Slovak Republic, KEGA, grant number 025ŽU-4/2024.

## References

Brandstetter, P., and Dobrovsky, M. (2013). *Speed Estimation of Induction Motor Using Model Reference Adaptive System with Kalman Filter*. Advances in Electrical and Electronic Engineering, 11(1), 22–28. doi:10.15598/aeee.v11i1.802.

Chen, B., Gao, C., Zhang, L., Chen, J., Chen, J. and Li, Y. (2023). Optimal Control Algorithm for Subway Train Operation by Proximal Policy Optimization. *Applied Science*, 13, p. 7456. doi: 10.3390/app13137456

Franke, R., Terwiesch, P. and Meyer, M. (2000). An Algorithm for the Optimal Control of the Driving of Train.

Ftorek, B., Saga, M., Orsansky, P., Vittek, J. and Butko, P. (2021). Energy Consumption Optimization for AC

Drives Position Control. *The International Journal for Computation and Mathematics in Electrical and Electronic Engineering*, 40(3), pp. 309–324. doi: 10.1108/COMPEL-10-2019-0429

Heineken, W., Richter, M. and Birth-Reichert, T. (2023). Energy-Efficient Train Driving Based on Optimal Control Theory. *Energies*, 16(18), p. 6712. doi: 10.3390/en16186712

Howlett, P. (2000). The Optimal Control of a Train. *Annals of Operations Research*, 98, pp. 65–87. doi: 10.1023/A:1019235819716

Ichikawa, K. (1968). Application of Optimization Theory for Bounded State Variable Problems to the Operation of Train. *Bulletin of Japanese Mechanical Engineering*, 11, pp. 857–865. doi: 10.1299/jsme1958.11.857

Novotny, D. W. and Lipo, T. A. (1996). *Vector Control and Dynamics of AC Drives*. Oxford: Clarendon Press.

Orlowska-Kowalska, T. and Dybkowski, M. (2016). Industrial Drive Systems. Current State and Development Trends. *Power Electronics and Drives*, 36(1), pp. 5–25. doi: 10.5277/PED160101

Perdukova, D., Fedor, P. and Timko, J. (2004). Modern Methods of Complex Drives Control. *Acta Technica CSAV*, 49(1), pp. 31–45. ISSN 0001-7043.

Ping, L. K., You, G. Z. and Hua, M. B. (2023). Energy Optimal Control Model for Train Movements. *Chinese Physics*, 16, p. 359. doi: 10.1088/1009-1963/16/2/015

Pontryagin, L. S. (2018) *Mathematical Theory of Optimal Processes*. Routledge, Abingdon-on-Thames. doi: 10.1201/9780203749319.

Su, S., Tang, T. and Wang, Y. (2016). Evaluation of Strategies to Reducing Traction Energy Consumption of Metro Systems Using an Optimal Train Control Simulation Model. *Energies*, 9(2), p. 105. doi: 10.3390/en9020105

Tolle, H. (1975). *Optimization Methods*. Berlin: Springer-Verlag.

Vittek, J., Butko, P., Ftorek, B., Makyš, P. and Gorel, L. (2017a). Energy Near-Optimal Control Strategies for Industrial and Traction Drives with A.C. Motors. *Mathematical Problems in Engineering*, 2017, pp. 1–22. doi: 10.1155/2017/1857186

Vittek, J., Gorel, L., Vavrúš, V. and Struharňanský, L. (2017b). Position Tracking Systems for AC Drives Employing Forced Dynamics Control. *Power Electronics and Drives*, 37(2), pp. 89–103. doi: 10.5277/PED170110

# Appendix

**Table A1.** IM nominal parameters.

| | | | | | | | |
|---|---|---|---|---|---|---|---|
| Nominal output power | $P_N$ | 720 | kW | Nominal frequency | $f_N$ | 50 | Hz |
| Nominal speed | $\omega_N$ | 156.24 | rads$^{-1}$ | Nominal voltage | $U_N$ | 780 | V |
| Nominal current | $I_N$ | 650 | A | Maximal current | $I_{max}$ | 810 | A |
| Nominal torque | $\Gamma_N$ | 4929 | Nm | Nominal power factor | $\cos\varphi_N$ | 0.88 | - |
| Pole-pairs number | $p$ | 2 | - | Total resistance | $R_c$ | 0.0952 | $\Omega$ |
| Stator resistance | $R_s$ | 0.0358 | $\Omega$ | Rotor resistance | $R_r$ | 0.032 | $\Omega$ |
| Mutual inductance | $L_m$ | 15.5 | mH | Leakage inductance | $L_\sigma$ | 12 | mH |
| Total mass | $M_u$ | 45.8 | t | Total moment of inertia | $J_r$ | 470 | kgm$^2$ |
| Wheel average diameter | $D_{wa}$ | 0.91 | m | Gear ratio | $u$ | 3.73 | - |